Structural Engineering and Mechanics, *Vol. 53, No. 3 (2015) 497-517*
DOI: http://dx.doi.org/10.12989/sem.2015.53.3.497

Temperature-dependent nonlocal nonlinear buckling analysis of functionally graded SWCNT-reinforced microplates embedded in an orthotropic elastomeric medium

Ali Akbar Mosallaie Barzoki*, Abbas Loghman and Ali Ghorbanpour Arani

Faculty of Mechanical Engineering, University of Kashan, Kashan, Iran

(Received July 30, 2014, Revised October 15, 2014, Accepted October 29, 2014)

Abstract. In this study, nonlocal nonlinear buckling analysis of embedded polymeric temperature-dependent microplates resting on an elastic matrix as orthotropic temperature-dependent elastomeric medium is investigated. The microplate is reinforced by single-walled carbon nanotubes (SWCNTs) in which the equivalent material properties nanocomposite are estimated based on the rule of mixture. For the carbon-nanotube reinforced composite (CNTRC) plate, both cases of uniform distribution (UD) and functionally graded (FG) distribution patterns of SWCNT reinforcements are considered. The small size effects of microplate are considered based on Eringen's nonlocal theory. Based on orthotropic Mindlin plate theory along with von Kármán geometric nonlinearity and Hamilton's principle, the governing equations are derived. Generalized differential quadrature method (GDQM) is applied for obtaining the buckling load of system. The effects of different parameters such as nonlocal parameters, volume fractions of SWCNTs, distribution type of SWCNTs in polymer, elastomeric medium, aspect ratio, boundary condition, orientation of foundation orthtotropy direction and temperature are considered on the nonlinear buckling of the microplate. Results indicate that CNT distribution close to top and bottom are more efficient than those distributed nearby the mid-plane for increasing the buckling load.

Keywords: nonlinear buckling; temperature-dependent; nanocomposite microplates; orthotropic elastomeric medium; FG materials

1. Introduction

Recently, due to the advantageous mechanical, physical and electronic properties of CNTs (Salvetat-Delmotte and Rubio 2002), these advanced materials are considered to be excellent candidates for the reinforcement of polymer composites (Esawi and Farag 2007, Fiedler *et al*. 2006). In actual structural applications, CNTRC, as a type of advanced material, have a wide variety of applications in microelectromechanical systems (MEMS) and nanoelectromechanical systems (NEMS). Hence, knowledge of the buckling characteristics of these structures is important. The traditional approach to fabricating nanocomposites implies that the nanotube is distributed either uniformly or randomly such that the resulting mechanical, thermal, or physical properties do not vary spatially at the macroscopic level. Functionally graded materials (FGMs)

*Corresponding author, Ph.D. Student , E-mail: amosallaiebarzoki@gmail.com

http://www.techno-press.org/?journal=sem&subpage=8 ISSN: 1225-4568 (Print), 1598-6217 (Online)

are a new generation of composite materials in which the microstructural details are spatially varied through nonuniform distribution of the reinforcement phase. The concept of FGM can be utilized for the management of a material's microstructure so that the bending behavior of a plate structure made of such material can be improved. These materials have found a wide range of applications in many industries (Shahba and Rajasekaran 2012, Wattanasakulpong *et al*. 2012).

The problem of buckling of thick plates has attracted considerable attention in recent years. Akhavan *et al*. (2009a, b) introduced exact solutions for the buckling analysis of rectangular Mindlin plates subjected to uniformly and linearly distributed in-plane loading on two opposite edges simply supported resting on elastic foundation. Flexural stability of a homogeneous plate compressed in its plane and lying on an elastic foundation was studied by Morozov and Tovstik (2010). Kim (2004) investigated the stability and dynamic displacement response of an infinite thin plate resting on a Winkler-type or a two-parameter elastic foundation when the system is subjected to in-plane static compressive forces. Postbuckling, nonlinear bending and nonlinear vibration analyses for SWCNTs resting on a two-parameter elastomeric foundation in thermal environments were presented by Shen and Zhang (2011).

None of the above researchers have considered nanocomposite structures. Reddy (1984) studied the effect of transverse shear deformation on deflection and stresses of laminated composite plates subjected to uniformly distributed load using finite element analyses. Analysis of composite plates using higher-order shear deformation theory and a finite point formulation based on the multiquadric radial basis function method was presented by Ferreira *et al*. (2003). Swaminathan and Ragounadin (2004) applied an analytical solution for static analyses of antisymmetric angle-ply composite and sandwich plates. An investigation on the nonlinear bending of simply supported, functionally graded nanocomposite plates reinforced by SWCNTs subjected to a transverse uniform or sinusoidal load in thermal environments was investigated by Shen (2009). Baltacıoğlu *et al*. (2011) presented the nonlinear static analysis of a rectangular laminated composite thick plate resting on nonlinear two-parameter elastic foundation with cubic nonlinearity. They used the first-order shear deformation theory for plate formulation and investigated the effects of foundation and geometric parameters of plates on nonlinear deflections. The mechanical buckling of a functionally graded nanocomposite rectangular plate reinforced by aligned and straight single-walled carbon nanotubes (SWCNTs) subjected to uniaxial and biaxial in-plane loadings was investigated by Jafari Mehrabadi *et al*. (2012).

None of the above studies have considered microplate nanocomposites. In micro scale, small size effects are important. Nonlocal elasticity theory was initiated in the papers of Eringen (1972). He regarded the stress state at a given point as a function of the strain states of all points in the body, while the local continuum mechanics assumes that the stress state at a given point depends uniquely on the strain state at the same point. Thermal buckling characteristics of rectangular flexural microplates subjected to uniform temperature were investigated by Farahmand *et al*. (2011) using higher continuity P-version finite element framework. Ahmadi *et al*. (2012) investigated elastic buckling of rectangular flexural micro plates using a higher continuity P-version finite-element framework based on Galerkin formulation.

In the present study, nonlocal nonlinear buckling behavior of polymeric temperature-dependent microplates reinforced by SWCNTs resting on orthotropic temperature-dependent elastomeric medium is investigated. For CNTRC plate, UD and three types of FG distribution patterns of SWCNT reinforcements are assumed. In order to obtain the equivalent material properties of FG-CNTRC plate, the rule of mixture is used. The nonlinear governing equations are obtained based on Hamilton's principal along with orthotropic Mindlin plate theory. GDQM is applied for

nonlinear buckling load of the FG-CNTRC polymeric microplate. The effects of the volume fractions of carbon nanotubes, elastomeric medium, aspect ratio, temperature, boundary conditions, orientation of foundation orthtotropy direction and applied force on the buckling load of the FG-CNTRC polymeric plate are discussed in detail.

2. Formulation

2.1 CNT-reinforced composite polymeric microplate

As shown in Fig. 1, a CNTRC microplate with length L_x, width L_y and thickness h is considered. The CNTRC plate is surrounded by an orthotropic elastomeric temperature-dependent medium which is simulated by K_W, G_ξ and G_η correspond Winkler foundation parameter, shear foundation parameters in ξ and η directions, respectively. Four types of CNTRC plates namely as uniform distribution (UD) along with three types of FG distributions (FGA, FGO, FGX) of CNTs along the thickness direction of a CNTRC plate is considered. In order to obtain the equivalent material properties two-phase Nanocomposites (i.e., polymer as matrix and CNT as reinforcer), the rule of mixture (Esawi and Farag 2007) is applied. According to mixture rule, the effective Young and shear moduli of CNTRC plate can be written as

$$E_{11} = \eta_1 V_{CNT} E_{r11} + (1 - V_{CNT}) E_m, \tag{1a}$$

$$\frac{\eta_2}{E_{22}} = \frac{V_{CNT}}{E_{r22}} + \frac{(1 - V_{CNT})}{E_m}, \tag{1b}$$

$$\frac{\eta_3}{G_{12}} = \frac{V_{CNT}}{G_{r12}} + \frac{(1 - V_{CNT})}{G_m}, \tag{1c}$$

where E_{r11}, E_{r22} and G_{r12} indicate the Young's moduli and shear modulus of SWCNTs, respectively, and E_m, G_m represent the corresponding properties of the isotropic matrix. The scale-dependent material properties, η_j (j=1, 2, 3), can be calculated by matching the effective properties of CNTRC obtained from the MD simulations with those from the rule of mixture. V_{CNT} and V_m are the volume fractions of the CNTs and matrix, respectively, which the sum of them equals to unity.

The uniform and three types of FG distributions of the CNTs along the thickness direction of the CNTRC plates take the following forms

$$UD: \quad V_{CNT} = V_{CNT}^*, \tag{2a}$$

$$FGV: \quad V_{CNT}(z) = \left(1 - \frac{2z}{h}\right) V_{CNT}^*, \tag{2b}$$

$$FGO: \quad V_{CNT}(z) = 2\left(1 - \frac{2|z|}{h}\right) V_{CNT}^*, \tag{2c}$$

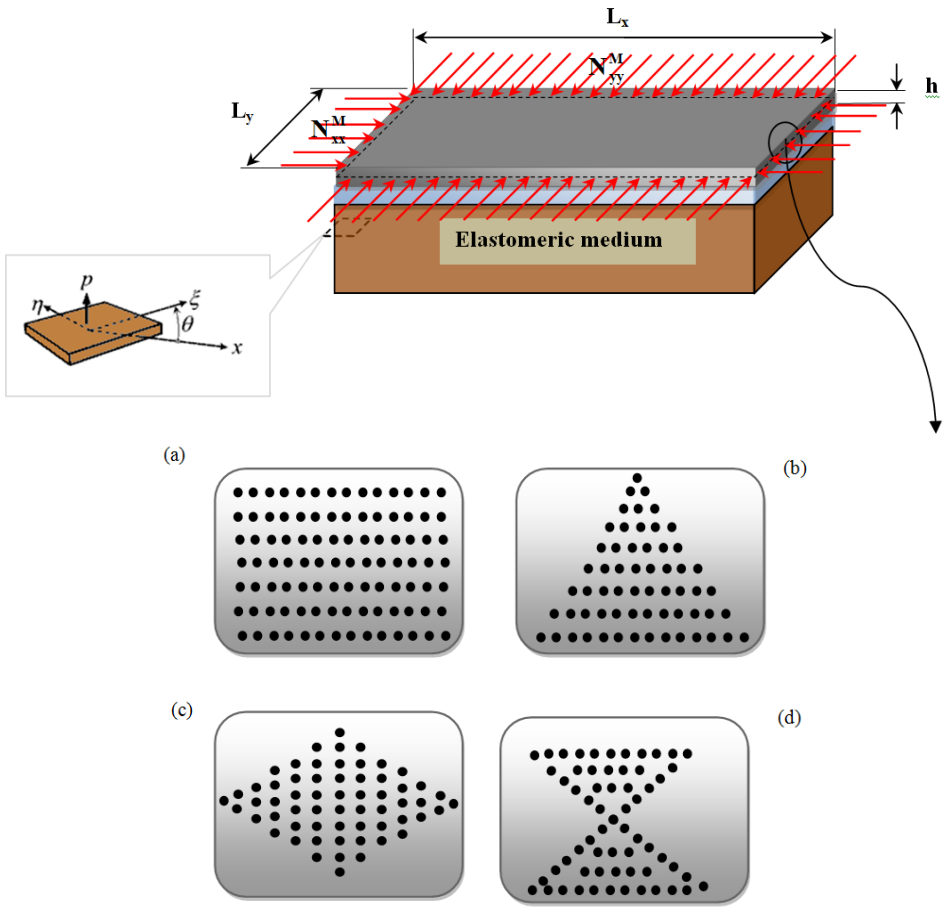

Fig. 1 Configurations of the SWCNT distribution in a CNTRC plates. (a) UD CNTRC plate; (b) FG-A CNTRC plate; (c) FG-O CNTRC plate; (d) FG-X CNTRC plate

$$FGX:\ V_{CNT}(z)=2\left(\frac{2|z|}{h}\right)V_{CNT}^{*}, \tag{2d}$$

where

$$V_{CNT}^{*}=\frac{w_{CNT}}{w_{CNT}+\left(\rho_{CNT}/\rho_{m}\right)-\left(\rho_{CNT}/\rho_{m}\right)w_{CNT}}, \tag{3}$$

where w_{CNT}, ρ_m and ρ_{CNT} are the mass fraction of the CNT, the densities of the matrix and CNT, respectively. Similarly, the thermal expansion coefficients in the longitudinal and transverse directions respectively (α_{11} and α_{22}), Poisson's ratio (ν_{11}) and the density (ρ) of the CNTRC plates can be determined as

$$\nu_{12}=V_{CNT}^{*}\nu_{r12}+V_{m,}\nu_{m}, \tag{4}$$

$$\rho = V_{CNT}^{*}\rho_r + V_{m,}\rho_{m,}, \tag{5}$$

$$\alpha_{11} = V_{CNT}^{*}\alpha_{r11} + V_{m,}\alpha_{m,}, \tag{6}$$

$$\alpha_{22} = (1+\nu_{r12})V_{CNT}\alpha_{r22} + (1+\nu_m)V_m\alpha_m - \nu_{12}\alpha_{11}, \tag{7}$$

where ν_{r12} and ν_m are Poisson's ratios of the CNT and matrix, respectively. In addition, α_{r11}, α_{r22} and α_m are the thermal expansion coefficients of the CNT and matrix, respectively. It should be noted that ν_{12} is assumed as constant over the thickness of the FG-CNTRC plates.

2.2 Orthotropic stress-strain relations

In the Eringen's nonlocal elasticity model, the stress state at a reference point in the body is regarded to be dependent not only on the strain state at this point but also on the strain states at all of the points throughout the body. The basic equations for homogeneous, isotropic and nonlocal elastic solid with zero body forces are given by Eringen (1972)

$$\begin{aligned} &\sigma_{ij,j} = 0 \\ &\sigma_{ij}(x) = \int \alpha(|x-x'|,\tau)\, C_{ijkl}\, \varepsilon_{kl}(x')\, dV(x'), \quad \forall x \in V \\ &\varepsilon_{ij} = \frac{1}{2}(u_{i,j} + u_{j,i} + u_{k,i}u_{k,j}) \end{aligned} \tag{8}$$

where, C_{ijkl} is the elastic module tensor of classical (local) isotropic elasticity; σ_{ij} and ε_{ij} are stress and strain tensors, respectively, and u_i is displacement vector. $\alpha(|x-x'|, \tau)$ is the nonlocal modulus. $|x-x'|$ is the Euclidean distance, and $\tau=e_0a/l$ is defined that l is the external characteristic length, e_0 denotes a constant appropriate to each material, and a is an internal characteristic length of the material (e.g., length of C-C bond, lattice spacing, granular distance). Consequently, e_0a is a constant parameter which is obtained with molecular dynamics, experimental results, experimental studies and molecular structure mechanics. The constitutive equation of the nonlocal elasticity can be written as

$$(1-(e_0a)^2\,\nabla^2)\sigma_{ij} = C_{ijkl}\,\varepsilon_{kl}, \tag{9}$$

where the parameter e_0a denotes the small scale effect on the response of structures in nanosize, and ∇^2 is the Laplace operator in the above equation.

The constitutive equation for stresses $\boldsymbol{\sigma}$ and strains $\boldsymbol{\varepsilon}$ matrix in thermal environment may be written as follows

$$\left(1-(e_0a)^2\nabla^2\right)\begin{Bmatrix}\sigma_{xx}\\ \sigma_{yy}\\ \sigma_{yz}\\ \sigma_{zx}\\ \sigma_{xy}\end{Bmatrix} = \begin{bmatrix} C_{11}(z,T) & C_{12}(z,T) & 0 & 0 & 0 \\ C_{21}(z,T) & C_{22}(z,T) & 0 & 0 & 0 \\ 0 & 0 & C_{44}(z,T) & 0 & 0 \\ 0 & 0 & 0 & C_{55}(z,T) & 0 \\ 0 & 0 & 0 & 0 & C_{66}(z,T) \end{bmatrix} \begin{Bmatrix} \varepsilon_{xx}-\alpha_{11}\Delta T \\ \varepsilon_{yy}-\alpha_{22}\Delta T \\ \gamma_{yz} \\ \gamma_{xz} \\ \gamma_{xy} \end{Bmatrix}, \tag{10}$$

where $C_{ij}(i,j=1,2,...,6)$ denotes temperature-dependent elastic coefficients which can be expressed as

$$C_{11} = E_{11}/(1-\nu_{12}\nu_{21}), C_{12} = \nu_{12}E_{12}/(1-\nu_{12}\nu_{21})$$
$$C_{22} = E_{22}/(1-\nu_{12}\nu_{21}) \tag{11}$$
$$C_{44} = G_{23}, C_{55} = G_{13}, C_{66} = G_{12}$$

Noted that C_{ij} and α_{11}, α_{22} may be obtained using rule of mixture (i.e., Eqs. (1)-(7)).

2.3 Nonlinear Mindlin plate theory

Based on Mindlin plate theory, the displacement field can be expressed as (Reddy 1984)

$$u_x(x,y,z,t) = u\ (x,y,t) + z\psi_x(x,y,t),$$
$$u_y(x,y,z,t) = v(x,y,t) + z\psi_y(x,y,t), \tag{12}$$
$$u_z(x,y,z,t) = w(x,y,t),$$

where (u_x, u_x, u_z) denote the displacement components at an arbitrary point (x,y,z) in the plate, and (u,v,w) are the displacement of a material point at (x,y) on the mid-plane (i.e., z=0) of the plate along the x-, y-, and z-directions, respectively; $\psi_x(x,y)$ and $\psi_y(x,y)$are the rotations of the normal to the mid-plane about x- and y- directions, respectively.

The von Kármán strains associated with the above displacement field can be expressed in the following form

$$\varepsilon_{xx} = \frac{\partial u}{\partial x} + \frac{1}{2}\left(\frac{\partial w}{\partial x}\right)^2 + z\frac{\partial \psi_x}{\partial x} \tag{13}$$

$$\varepsilon_{yy} = \frac{\partial v}{\partial y} + \frac{1}{2}\left(\frac{\partial w}{\partial y}\right)^2 + z\frac{\partial \psi_y}{\partial y} \tag{14}$$

$$\gamma_{yz} = \frac{\partial w}{\partial y} + \psi_y \tag{15}$$

$$\gamma_{xz} = \frac{\partial w}{\partial x} + \psi_x \tag{16}$$

$$\gamma_{xy} = \frac{\partial v}{\partial y} + \frac{\partial u}{\partial x} + \frac{\partial w}{\partial x}\frac{\partial w}{\partial y} + z\left(\frac{\partial \psi_x}{\partial y} + \frac{\partial \psi_y}{\partial x}\right), \tag{17}$$

where (ε_{xx}, ε_{yy}) are the normal strain components and (γ_{yz}, γ_{xz}, γ_{xy}) are the shear strain components.

2.4 Energy method

The total potential energy, *V*, of the CNTRC plate is the sum of strain energy, *U* and the work done by the elasomeric medium, *W*.

2.4.1 Potential energy

The strain energy can be written as

$$U = \frac{1}{2}\int_{\Omega_0}\int_{-h/2}^{h/2}\left(\sigma_{xx}\varepsilon_{xx} + \sigma_{yy}\varepsilon_{yy} + \sigma_{xy}\gamma_{xy} + \sigma_{xz}\gamma_{xz} + \sigma_{yz}\gamma_{yz}\right)dV\,, \tag{18}$$

Combining of Eqs. (10)- (17) yields

$$\begin{aligned} U = \frac{1}{2}\int_{\Omega_0}\Bigg(& N_{xx}\left(\frac{\partial u}{\partial x} + \frac{1}{2}\left(\frac{\partial w}{\partial x}\right)^2\right) + N_{yy}\left(\frac{\partial v}{\partial y} + \frac{1}{2}\left(\frac{\partial w}{\partial y}\right)^2\right) + N_{yz}\left(\frac{\partial w_0}{\partial y} + \psi_y\right) + N_{xz}\left(\frac{\partial w_0}{\partial x} + \psi_x\right) \\ & + N_{xy}\left(\frac{\partial v}{\partial y} + \frac{\partial u}{\partial x} + \frac{\partial w}{\partial x}\frac{\partial w}{\partial y}\right) + M_{xx}\frac{\partial \psi_x}{\partial x} + M_{yy}\frac{\partial \psi_y}{\partial x} + M_{xy}\left(\frac{\partial \psi_x}{\partial y} + \frac{\partial \psi_y}{\partial x}\right)\Bigg)dxdy \end{aligned} \tag{19}$$

where the stress resultant-displacement relations can be written as

$$\begin{bmatrix} N_{xx} & M_{xx} \\ N_{yy} & M_{yy} \\ N_{xy} & M_{xy} \end{bmatrix} = \int_{-h/2}^{h/2}\begin{bmatrix} \sigma_{xx} \\ \sigma_{yy} \\ \sigma_{xy} \end{bmatrix}(1, z)dz, \tag{20}$$

$$\begin{bmatrix} N_{xz} \\ N_{yz} \end{bmatrix} = K\int_{-h/2}^{h/2}\begin{bmatrix} \sigma_{xz} \\ \sigma_{yz} \end{bmatrix}dz, \tag{21}$$

In which *K* is shear correction coefficient.

2.4.2 External work

The external work due to orthotropic temperature-dependent elastomeric medium and a uniform load on upper surface of the CNTRC plate can be written as

$$W = \int_0^L (P + q)w dx, \tag{22}$$

where *P* and *q* are related to orthotropic elastomeric medium and distributed load on upper surface of the plate, respectively. Orthotropic elastomeric foundation can be expressed as (Shen 2009, Kutlu and Omurtag 2012)

$$\begin{aligned} P = {} & K_W w - G_\xi\left(\cos^2\theta w_{,xx} + 2\cos\theta\sin\theta w_{,yx} + \sin^2\theta w_{,yy}\right) \\ & - G_\eta\left(\sin^2\theta w_{,xx} - 2\sin\theta\cos\theta w_{,yx} + \cos^2\theta w_{,yy}\right), \end{aligned} \tag{23}$$

where angle θ describes the local ξ direction of orthotropic foundation with respect to the global *x*-

axis of the plate. Since the elastomeric medium is relatively soft, the foundation stiffness k may be expressed by

$$k = \frac{E_0}{4L(1-\nu_0^2)(2-c_1)^2}\left[5-\left(2\gamma_1^2+6\gamma_1+5\right)\exp\left(-2\gamma_1\right)\right], \tag{24}$$

where

$$c_1 = \left(\gamma_1+2\right)\exp\left(-\gamma_1\right), \tag{25}$$

$$\gamma_1 = \frac{H_s}{L}, \tag{26}$$

$$E_0 = \frac{E_s}{\left(1-\nu_s^2\right)}, \tag{27}$$

$$\nu_0 = \frac{\nu_s}{\left(1-\nu_s\right)}, \tag{28}$$

where E_s, ν_s, H_s are Young's modulus, Poisson's ratio and depth of the foundation, respectively. In this paper, E_s is assumed to be temperature-dependent while ν_s is assumed to be a constant (Swaminathan and Ragounadin 2004).

2.5 Governing equations

The governing equations can be derived by Hamilton's principal as follows

$$\delta\int_0^t(-U+W)dt=0 \Rightarrow \int_0^t(-\delta U+\delta W)dt=0. \tag{29}$$

Substituting Eqs. (19) and (22) into Eq. (29) yields the following governing equations

$$\delta u:\frac{\partial N_{xx}}{\partial x}+\frac{\partial N_{xy}}{\partial y}=0, \tag{30}$$

$$\delta v:\frac{\partial N_{xy}}{\partial x}+\frac{\partial N_{yy}}{\partial y}=0, \tag{31}$$

$$\delta w:\frac{\partial N_{xz}}{\partial x}+\frac{\partial N_{yz}}{\partial y}+\frac{\partial}{\partial x}\left(N_{xx}\frac{\partial w}{\partial x}+N_{xy}\frac{\partial w}{\partial y}\right)+\frac{\partial}{\partial y}\left(N_{xy}\frac{\partial w}{\partial x}+N_{yy}\frac{\partial w}{\partial y}\right)+P=0. \tag{32}$$

$$\delta\psi_x:\frac{\partial M_{xx}}{\partial x}+\frac{\partial M_{xy}}{\partial y}-N_{xz}=0, \tag{33}$$

$$\delta\psi_y:\frac{\partial M_{xy}}{\partial x}+\frac{\partial M_{yy}}{\partial y}-N_{yz}=0, \tag{34}$$

Substituting Eqs. (10) and (13)-(17) into Eqs. (20) and (21), the stress resultant-displacement relations can be obtained as follow

$$\begin{Bmatrix} N_{xx} \\ N_{yy} \\ N_{yz} \\ N_{xz} \\ N_{xy} \end{Bmatrix} = \left(1-(e_0a)^2\nabla^2\right)\begin{bmatrix} A_{11} & A_{12} & 0 & 0 & 0 \\ A_{12} & A_{22} & 0 & 0 & 0 \\ 0 & 0 & A_{44} & 0 & 0 \\ 0 & 0 & 0 & A_{55} & 0 \\ 0 & 0 & 0 & 0 & A_{66} \end{bmatrix}\begin{Bmatrix} \dfrac{\partial u}{\partial x}+\dfrac{1}{2}\left(\dfrac{\partial w}{\partial x}\right)^2 \\ \dfrac{\partial v}{\partial y}+\dfrac{1}{2}\left(\dfrac{\partial w}{\partial y}\right)^2 \\ \dfrac{\partial w}{\partial y}+\psi_y \\ \dfrac{\partial w}{\partial x}+\psi_x \\ \dfrac{\partial u}{\partial y}\dfrac{\partial v}{\partial x}+\dfrac{\partial w}{\partial x}\dfrac{\partial w}{\partial y} \end{Bmatrix} - \begin{Bmatrix} N_{xx}^T \\ N_{yy}^T \\ 0 \\ 0 \\ 0 \end{Bmatrix}, \tag{35}$$

$$\begin{Bmatrix} M_{xx} \\ M_{yy} \\ M_{xy} \end{Bmatrix} = \left(1-(e_0a)^2\nabla^2\right)\begin{bmatrix} D_{11} & D_{12} & 0 \\ D_{12} & D_{22} & 0 \\ 0 & 0 & D_{66} \end{bmatrix}\begin{Bmatrix} \dfrac{\partial \psi_x}{\partial x} \\ \dfrac{\partial \psi_y}{\partial y} \\ \dfrac{\partial \psi_x}{\partial y}+\dfrac{\partial \psi_y}{\partial x} \end{Bmatrix} - \begin{Bmatrix} M_{xx}^T \\ M_{yy}^T \\ 0 \end{Bmatrix}, \tag{36}$$

where

$$A_{ij} = \int_{-h/2}^{h/2} C_{ij}\,dz, \qquad (i,j=1,2,6) \tag{37}$$

$$\left(A_{44}, A_{55}\right) = \int_{-h/2}^{h/2} K\left(G_{23}, G_{13}\right)dz, \tag{38}$$

$$D_{ij} = \int_{-h/2}^{h/2} C_{ij}\,z\,dz, \tag{39}$$

Furthermore, $\left(N_{xx}^T, N_{yy}^T\right)$ and $\left(M_{xx}^T, M_{yy}^T\right)$ are thermal force and thermal moment resultants, respectively, and are given by

$$\begin{Bmatrix} N_{xx}^T \\ N_{yy}^T \end{Bmatrix} = \int_{-h/2}^{h/2} \begin{Bmatrix} C_{11}(z,T)\alpha_{11}+C_{12}(z,T)\alpha_{22} \\ C_{21}(z,T)\alpha_{11}+C_{22}(z,T)\alpha_{22} \end{Bmatrix}\Delta T\,dz, \tag{40}$$

$$\begin{Bmatrix} M_{xx}^T \\ M_{yy}^T \end{Bmatrix} = \int_{-h/2}^{h/2} \begin{Bmatrix} C_{11}(z,T)\alpha_{11}+C_{12}(z,T)\alpha_{22} \\ C_{21}(z,T)\alpha_{11}+C_{22}(z,T)\alpha_{22} \end{Bmatrix}\Delta T\,z\,dz, \tag{41}$$

Substituting Eqs. (35)-(41) into Eqs. (30)-(34), the governing equations can be written as follow

$$\delta u: A_{11}\left(\frac{\partial^2 u}{\partial x^2}+\frac{\partial w}{\partial x}\frac{\partial^2 w}{\partial x^2}\right)+A_{12}\left(\frac{\partial^2 v}{\partial x\partial y}+\frac{\partial w}{\partial y}\frac{\partial^2 w}{\partial x\partial y}\right)+A_{66}\left(\frac{\partial^2 u}{\partial y^2}+\frac{\partial^2 v}{\partial x\partial y}+\frac{\partial w}{\partial y}\frac{\partial^2 w}{\partial x\partial y}+\frac{\partial w}{\partial x}\frac{\partial^2 w}{\partial y^2}\right)=0, \tag{42}$$

$$\delta v: A_{12}\left(\frac{\partial^2 u}{\partial x\partial y}+\frac{\partial w}{\partial x}\frac{\partial^2 w}{\partial x\partial y}\right)+A_{22}\left(\frac{\partial^2 v}{\partial y^2}+\frac{\partial w}{\partial y}\frac{\partial^2 w}{\partial y^2}\right)+A_{66}\left(\frac{\partial^2 v}{\partial x^2}+\frac{\partial^2 u}{\partial x\partial y}+\frac{\partial w}{\partial y}\frac{\partial^2 w}{\partial x^2}+\frac{\partial w}{\partial x}\frac{\partial^2 w}{\partial x\partial y}\right)=0, \tag{43}$$

$$\begin{aligned}\delta w: & A_{55}\left(\frac{\partial \psi_x}{\partial x}+\frac{\partial^2 w}{\partial x^2}\right)+A_{44}\left(\frac{\partial \psi_y}{\partial y}+\frac{\partial^2 w}{\partial y^2}\right)\\ &+\left(1-(e_0 a)^2\nabla^2\right)\begin{pmatrix}\left(N_{xx}^T+\chi_1 N_{xx}^M\right)\frac{\partial^2 w}{\partial x^2}+\left(N_{yy}^T+\chi_2 N_{yy}^M\right)\frac{\partial^2 w}{\partial y^2}+kw\\ -G_\xi\left(\cos^2\theta w_{,xx}+2\cos\theta\sin\theta w_{,yx}+\sin^2\theta w_{,yy}\right)\\ -G_\eta\left(\sin^2\theta w_{,xx}-2\sin\theta\cos\theta w_{,yx}+\cos^2\theta w_{,yy}\right)\end{pmatrix}=0,\end{aligned} \tag{44}$$

$$\delta\psi_x: D_{11}\frac{\partial^2\psi_x}{\partial x^2}+D_{12}\frac{\partial^2\psi_y}{\partial x\partial y}+D_{66}\left(\frac{\partial^2\psi_x}{\partial y^2}+\frac{\partial^2\psi_y}{\partial x\partial y}\right)-A_{55}\left(\psi_x+\frac{\partial w}{\partial x}\right)=0, \tag{45}$$

$$\delta\psi_y: D_{12}\frac{\partial^2\psi_x}{\partial x\partial y}+D_{22}\frac{\partial^2\psi_y}{\partial y^2}+D_{66}\left(\frac{\partial^2\psi_y}{\partial x^2}+\frac{\partial^2\psi_x}{\partial x\partial y}\right)-A_{44}\left(\psi_y+\frac{\partial w}{\partial y}\right)=0. \tag{46}$$

The CNTRC micro-plates are considered with three kinds of boundary conditions: all edges simply supported (SSSS) or clamped (CCCC), and two opposite edges simply supported and the other two clamped (SCSC). The boundary conditions are given as follows:

SSSS

$$x=0,L_x \Rightarrow v=w=\psi_y=0, \tag{47}$$

$$y=0,L_y \Rightarrow u=w=\psi_x=0. \tag{48}$$

CCCC

$$x=0,L_x \Rightarrow v=w=\psi_x=\psi_y=0, \tag{49}$$

$$y=0,L_y \Rightarrow u=w=\psi_x=\psi_y=0. \tag{50}$$

SCSC

$$x=0,L_x \Rightarrow v=w=\psi_y=0, \tag{51}$$

$$y=0,L_y \Rightarrow u=w=\psi_x=\psi_y=0. \tag{52}$$

3. GDQM

There is a lot of numerical method to solve the initial-and/or boundary value problems which occur in engineering domain. Some of the common numerical methods are FEM, Galerkin method, finite difference method (FDM), GDQM and etc. FEM and FDM for higher-order modes require to a great number of grid points. Therefore these solution methods for all these points need to more CPU time, while the GDQM has several benefits that are listed as below (Chen 1996, Shu 1999, Civalek 2004):

1. GDQM is a powerful method which can be used to solve numerical problems in the analysis of structural and dynamical systems.
2. The accuracy and convergence of the GDQM is higher than FEM.
3. GDQM is an accurate method for solution of nonlinear differential equations in approximation of the derivatives.
4. This method can easily and exactly satisfy a variety of boundary conditions and require much less formulation and programming effort.
5. Recently, GDQM has been extended to handle irregular shaped.

Due to the above striking merits of the GDQM, in recent years the method has become increasingly popular in the numerical solution of problems in engineering and physical science. In this method, the differential equations are changed into a first order algebraic equation by employing appropriate weighting coefficients. Because weighting coefficients do not relate to any special problem and only depend on the grid spacing. In other words, the partial derivatives of a function (say w here) are approximated with respect to specific variables (say x and y), at a discontinuous point in a defined domain ($0<x<L_x$ and $0<y<L_y$) as a set of linear weighting coefficients and the amount represented by the function itself at that point and other points throughout the domain. The approximation of the n^{th} and m^{th} derivatives function with respect to x and y, respectively may be expressed in general form as (Civalek 2004)

$$\begin{aligned} f_x^{(n)}(x_i,y_i) &= \sum_{k=1}^{N_x} A^{(n)}_{ik} f(x_k,y_j), \\ f_y^{(m)}(x_i,y_i) &= \sum_{l=1}^{N_y} B^{(m)}_{jl} f(x_i,y_l), \\ f_{xy}^{(n+m)}(x_i,y_i) &= \sum_{k=1}^{N_x} \sum_{l=1}^{N_y} A^{(n)}_{ik} B^{(m)}_{jl} f(x_k,y_l), \end{aligned} \tag{53}$$

where N_x and N_y, denotes the number of points in x and y directions, $f(x,y)$ is the function and A_{ik}, B_{jl} are the weighting coefficients defined as Civalek (2004)

$$\begin{aligned} A^{(1)}_{ij} &= \frac{M(x_i)}{(x_i-x_j)M(x_j)}, \\ B^{(1)}_{ij} &= \frac{P(y_i)}{(y_i-y_j)M(y_j)}, \end{aligned} \tag{54}$$

where M and P are Lagrangian operators defined as

$$M(x_i)=\prod_{j=1}^{N_x}(x_i-x_j),\ \ i\neq j$$
$$P(y_i)=\prod_{j=1}^{N_y}(y_i-y_j),\ \ i\neq j. \tag{55}$$

The weighting coefficients for the second, third and fourth derivatives are determined via matrix multiplication

$$A^{(2)}{}_{ij}=\sum_{k=1}^{N_x}A^{(1)}{}_{ik}A^{(1)}{}_{kj},\ \ A^{(3)}{}_{ij}=\sum_{k=1}^{N_x}A^{(2)}{}_{ik}A^{(1)}{}_{kj},\ \ A^{(4)}{}_{ij}=\sum_{k=1}^{N_x}A^{(3)}{}_{ik}A^{(1)}{}_{kj},\quad i,j=1,2,...,N_x,$$
$$B^{(2)}{}_{ij}=\sum_{k=1}^{N_y}B^{(1)}{}_{ik}B^{(1)}{}_{kj},\ \ B^{(3)}{}_{ij}=\sum_{k=1}^{N_y}B^{(2)}{}_{ik}B^{(1)}{}_{kj},\ \ B^{(4)}{}_{ij}=\sum_{k=1}^{N_y}B^{(3)}{}_{ik}B^{(1)}{}_{kj},\quad i,j=1,2,...,N_y. \tag{56}$$

Using the following rule, the distribution of grid points in domain is calculated as (Civalek 2004)

$$x_i=\frac{L_x}{2}[1-\cos(\frac{\pi i}{N_x})],$$
$$y_j=\frac{L_y}{2}[1-\cos(\frac{\pi j}{N_y})], \tag{57}$$

Substituting Eq. (53) into the governing equations turns it into a set of algebraic equations expressed as

$$\begin{aligned}
\delta u:\ & A_{11}\left(\sum_{k=1}^{N_x}A^{(2)}{}_{ik}u(x_k,y_j)+\sum_{k=1}^{N_x}A^{(1)}{}_{ik}w(x_k,y_j)\sum_{k=1}^{N_x}A^{(2)}{}_{ik}w(x_k,y_j)\right)\\
&+A_{12}\left(\sum_{k=1}^{N_x}\sum_{l=1}^{N_y}A^{(1)}{}_{ik}B^{(1)}{}_{jl}v(x_k,y_l)+\sum_{l=1}^{N_y}B^{(1)}{}_{jl}w(x_i,y_l)\sum_{k=1}^{N_x}\sum_{l=1}^{N_y}A^{(1)}{}_{ik}B^{(1)}{}_{jl}w(x_k,y_l)\right)\\
&+A_{66}\left(\sum_{l=1}^{N_y}B^{(2)}{}_{jl}u(x_i,y_l)+\sum_{k=1}^{N_x}\sum_{l=1}^{N_y}A^{(1)}{}_{ik}B^{(1)}{}_{jl}v(x_k,y_l)\right.\\
&\left.+\sum_{l=1}^{N_y}B^{(1)}{}_{jl}w(x_i,y_l)\sum_{k=1}^{N_x}\sum_{l=1}^{N_y}A^{(1)}{}_{ik}B^{(1)}{}_{jl}w(x_k,y_l)+\sum_{k=1}^{N_x}A^{(1)}{}_{ik}w(x_k,y_j)\sum_{l=1}^{N_y}B^{(2)}{}_{jl}w(x_i,y_l)\right)=0,
\end{aligned} \tag{58}$$

$$\begin{aligned}
\delta v:\ & A_{12}\left(\sum_{k=1}^{N_x}\sum_{l=1}^{N_y}A^{(1)}{}_{ik}B^{(1)}{}_{jl}u(x_k,y_l)+\sum_{k=1}^{N_x}A^{(1)}{}_{ik}w(x_k,y_j)\sum_{k=1}^{N_x}\sum_{l=1}^{N_y}A^{(1)}{}_{ik}B^{(1)}{}_{jl}w(x_k,y_l)\right)\\
&+A_{22}\left(\sum_{l=1}^{N_y}B^{(2)}{}_{jl}v(x_i,y_l)+\sum_{l=1}^{N_y}B^{(1)}{}_{jl}w(x_i,y_l)\sum_{l=1}^{N_y}B^{(2)}{}_{jl}w(x_i,y_l)\right)\\
&+A_{66}\left(\sum_{k=1}^{N_x}A^{(2)}{}_{ik}v(x_k,y_j)+\sum_{k=1}^{N_x}\sum_{l=1}^{N_y}A^{(1)}{}_{ik}B^{(1)}{}_{jl}u(x_k,y_l)+\sum_{l=1}^{N_y}B^{(1)}{}_{jl}w(x_i,y_l)\sum_{k=1}^{N_x}A^{(2)}{}_{ik}w(x_k,y_j)\right.\\
&\left.+\sum_{k=1}^{N_x}A^{(1)}{}_{ik}w(x_k,y_j)\sum_{k=1}^{N_x}\sum_{l=1}^{N_y}A^{(1)}{}_{ik}B^{(1)}{}_{jl}w(x_k,y_l)\right)=0,
\end{aligned} \tag{59}$$

$$
\begin{aligned}
&\delta w: A_{55}\left(\sum_{k=1}^{N_x} A^{(1)}{}_{ik}\psi_x(x_k,y_j)+\sum_{k=1}^{N_x} A^{(2)}{}_{ik}\,w(x_k,y_j)\right)+A_{44}\left(\sum_{l=1}^{N_y} B^{(1)}{}_{jl}\psi_y(x_k,y_l)+\sum_{l=1}^{N_y} B^{(2)}{}_{jl}w(x_i,y_l)\right)\\
&\left(1-(e_0a)^2\nabla^2\right)\left(\begin{array}{l}
+\left(N_{xx}^T+\chi_1 N_{xx}^M\right)\sum_{k=1}^{N_x} A^{(2)}{}_{ik}\,w(x_k,y_j)+\left(N_{yy}^T+\chi_2 N_{yy}^M\right)\sum_{l=1}^{N_y} B^{(2)}{}_{jl}w(x_i,y_l)+kw(x_i,y_j)\\
-G_\xi\left(\cos^2\theta\sum_{k=1}^{N_x} A^{(2)}{}_{ik}\,w(x_k,y_j)+2\cos\theta\sin\theta\sum_{k=1}^{N_x}\sum_{l=1}^{N_y} A^{(1)}{}_{ik}B^{(1)}{}_{jl}\,w(x_k,y_l)+\sin^2\theta\sum_{l=1}^{N_y} B^{(2)}{}_{jl}w(x_i,y_l)\right)\\
-G_\eta\left(\sin^2\theta\sum_{k=1}^{N_x} A^{(2)}{}_{ik}\,w(x_k,y_j)-2\sin\theta\cos\theta\sum_{k=1}^{N_x}\sum_{l=1}^{N_y} A^{(1)}{}_{ik}B^{(1)}{}_{jl}\,w(x_k,y_l)+\cos^2\theta\sum_{l=1}^{N_y} B^{(2)}{}_{jl}w(x_i,y_l)\right)
\end{array}\right)=0,
\end{aligned}
\tag{60}
$$

$$
\begin{aligned}
&\delta\psi_x: D_{11}\sum_{k=1}^{N_x} A^{(2)}{}_{ik}\,\psi_x(x_k,y_j)+D_{12}\sum_{k=1}^{N_x}\sum_{l=1}^{N_y} A^{(1)}{}_{ik}B^{(1)}{}_{jl}\psi_y(x_k,y_l)\\
&+D_{66}\left(\sum_{l=1}^{N_y} B^{(2)}{}_{jl}\psi_x(x_i,y_l)+\sum_{k=1}^{N_x}\sum_{l=1}^{N_y} A^{(1)}{}_{ik}B^{(1)}{}_{jl}\psi_y(x_k,y_l)\right)-A_{55}\left(\psi_x+\sum_{k=1}^{N_x} A^{(1)}{}_{ik}\,w(x_k,y_j)\right)=0,
\end{aligned}
\tag{61}
$$

$$
\begin{aligned}
&\delta\psi_y: D_{12}\sum_{k=1}^{N_x}\sum_{l=1}^{N_y} A^{(1)}{}_{ik}B^{(1)}{}_{jl}\psi_x(x_k,y_l)+D_{22}\sum_{l=1}^{N_y} B^{(2)}{}_{jl}\psi_y(x_i,y_l)\\
&+D_{66}\left(\sum_{k=1}^{N_x} A^{(2)}{}_{ik}\psi_y(x_k,y_j)+\sum_{k=1}^{N_x}\sum_{l=1}^{N_y} A^{(1)}{}_{ik}B^{(1)}{}_{jl}\psi_x(x_k,y_l)\right)-A_{44}\left(\psi_y+\sum_{l=1}^{N_y} B^{(1)}{}_{jl}w(x_i,y_l)\right)=0.
\end{aligned}
\tag{62}
$$

Finally, the governing equations (i.e., Eqs. (58)-(62)) in matrix form can be expressed as

$$
\left\{
\begin{bmatrix}
[KL_{1u}]_{N_xN_y\times N_xN_y} & [KL_{1v}]_{N_xN_y\times N_xN_y} & [0]_{N_xN_y\times N_xN_y} & [0]_{N_xN_y\times N_xN_y} & [0]_{N_xN_y\times N_xN_y}\\
[KL_{2u}]_{N_xN_y\times N_xN_y} & [KL_{2v}]_{N_xN_y\times N_xN_y} & [0]_{N_xN_y\times N_xN_y} & [0]_{N_xN_y\times N_xN_y} & [0]_{N_xN_y\times N_xN_y}\\
[0]_{N_xN_y\times N_xN_y} & [0]_{N_xN_y\times N_xN_y} & [KL_{3w}]_{N_xN_y\times N_xN_y} & [KL_{3\psi_x}]_{N_xN_y\times N_xN_y} & [KL_{3\psi_y}]_{N_xN_y\times N_xN_y}\\
[0]_{N_xN_y\times N_xN_y} & [0]_{N_xN_y\times N_xN_y} & [0]_{N_xN_y\times N_xN_y} & [KL_{4\psi_x}]_{N_xN_y\times N_xN_y} & [KL_{4\psi_y}]_{N_xN_y\times N_xN_y}\\
[0]_{N_xN_y\times N_xN_y} & [0]_{N_xN_y\times N_xN_y} & [KL_{5w}]_{N_xN_y\times N_xN_y} & [KL_{5\psi_x}]_{N_xN_y\times N_xN_y} & [KL_{5\psi_y}]_{N_xN_y\times N_xN_y}
\end{bmatrix}_{5N_xN_y\times 5N_xN_y}
+
\begin{bmatrix}
[0]_{N_xN_y\times N_xN_y} & [0]_{N_xN_y\times N_xN_y} & [KNL_{1w}]_{N_xN_y\times N_xN_y} & [0]_{N_xN_y\times N_xN_y} & [0]_{N_xN_y\times N_xN_y}\\
[0]_{N_xN_y\times N_xN_y} & [0]_{N_xN_y\times N_xN_y} & [KNL_{2w}]_{N_xN_y\times N_xN_y} & [0]_{N_xN_y\times N_xN_y} & [0]_{N_xN_y\times N_xN_y}\\
[0]_{N_xN_y\times N_xN_y} & [0]_{N_xN_y\times N_xN_y} & [0]_{N_xN_y\times N_xN_y} & [0]_{N_xN_y\times N_xN_y} & [0]_{N_xN_y\times N_xN_y}\\
[0]_{N_xN_y\times N_xN_y} & [0]_{N_xN_y\times N_xN_y} & [0]_{N_xN_y\times N_xN_y} & [0]_{N_xN_y\times N_xN_y} & [0]_{N_xN_y\times N_xN_y}\\
[0]_{N_xN_y\times N_xN_y} & [0]_{N_xN_y\times N_xN_y} & [0]_{N_xN_y\times N_xN_y} & [0]_{N_xN_y\times N_xN_y} & [0]_{N_xN_y\times N_xN_y}
\end{bmatrix}_{5N_xN_y\times 5N_xN_y}
\right\}
\begin{bmatrix}
[u]_{N_xN_y\times 1}\\ [v]_{N_xN_y\times 1}\\ [w]_{N_xN_y\times 1}\\ [\psi_x]_{N_xN_y\times 1}\\ [\psi_y]_{N_xN_y\times 1}
\end{bmatrix}_{5N_xN_y\times 1}
=
\begin{bmatrix}
[0]_{N_xN_y\times 1}\\ [0]_{N_xN_y\times 1}\\ [Q]_{N_xN_y\times 1}\\ [0]_{N_xN_y\times 1}\\ [0]_{N_xN_y\times 1}
\end{bmatrix}_{5N_xN_y\times 1},
\tag{63}
$$

where $[KL]$ and $[KNL]$ are respectively, linear and nonlinear coefficients which can be defined as

$$KL_{1u}=A_{11}A^{(2)}+A_{66}B^{(2)}, \tag{64a}$$

$$KL_{1v}=A_{12}A^{(1)}B^{(1)}+A_{66}A^{(1)}B^{(1)}, \tag{64b}$$

$$KL_{2u}=A_{12}A^{(1)}B^{(1)}+A_{66}A^{(1)}B^{(1)}, \tag{64c}$$

$$KL_{2v}=A_{22}B^{(2)}+A_{66}A^{(2)}, \tag{64d}$$

$$KL_{3w} = A_{55}A^{(2)} + A_{44}B^{(2)} + \left(N_{xx}^{T} + \chi_1 N_{xx}^{M}\right)A^{(2)} + \left(N_{yy}^{T} + \chi_2 N_{yy}^{M}\right)B^{(2)} + \left(1-(e_0 a)^2\nabla^2\right)\begin{pmatrix} +k - G_{\xi}\left(\cos^2\theta\, A^{(2)} + 2\cos\theta\sin\theta\, A^{(1)}B^{(1)}\right. \\ \left. +\sin^2\theta\, B^{(2)}\right) - G_{\eta}\left(\sin^2\theta\, A^{(2)} - 2\sin\theta\cos\theta\, A^{(1)}B^{(1)} + \cos^2\theta B^{(2)}\right)\end{pmatrix}, \tag{64e}$$

$$KL_{3\psi_x} = A_{55}A^{(1)}, \tag{64f}$$

$$KL_{3\psi_y} = A_{44}B^{(1)}, \tag{64g}$$

$$KL_{4\psi_x} = D_{11}A^{(2)} + D_{66}B^{(2)} - A_{55}, \tag{64h}$$

$$KL_{4\psi_y} = D_{12}A^{(1)}B^{(1)} + D_{66}A^{(1)}B^{(1)} - A_{55}A^{(1)}, \tag{64i}$$

$$KL_{5w} = -A_{44}B^{(1)}, \tag{64j}$$

$$KL_{5\psi_x} = D_{12}A^{(1)}B^{(1)} + D_{66}A^{(1)}B^{(1)}, \tag{64k}$$

$$KL_{5\psi_y} = D_{22}B^{(2)} + D_{66}A^{(2)} - A_{44}, \tag{64l}$$

$$KNL_{1w} = A_{11}A^{(1)}WA^{(2)} + A_{12}B^{(1)}WA^{(1)}B^{(1)} + A_{66}\left(B^{(1)}WA^{(1)}B^{(1)} + A^{(1)}WB^{(2)}\right), \tag{64m}$$

$$KNL_{2w} = A_{12}A^{(1)}WA^{(1)}B^{(1)} + A_{22}B^{(1)}WB^{(2)} + A_{66}\left(B^{(1)}WA^{(2)} + A^{(1)}WA^{(1)}B^{(1)}\right), \tag{64n}$$

The above nonlinear equation can now be solved using a direct iterative process as follows:

- First, nonlinearity is ignored by taking KNL=0 to solve Eq. (63). This yields the linear buckling load and deflection. The deflection is then scaled up.
- Using linear deflection, [KNL] could be evaluated. The problem is then solved by substituting [KNL] into Eq. (63). This would give the nonlinear deflection and buckling load.
- The new nonlinear deflection is scaled up again and the above procedure is repeated iteratively until the difference between deflection values from the two subsequent iterations becomes less than 0.01%.

4. Numerical results and discussion

A computer program is prepared for the numerical solution of nonlinear buckling of CNTRC plates resting on an orthotropic elastomeric temperature-dependent foundation. Here, Poly methyl methacrylate (PMMA) is selected for the matrix which have constant Poisson's ratios of ν_m=0.34, temperature-dependent thermal coefficient of α_m=(1+0.0005ΔT)×10^{-6}/K, and temperature-dependent Young moduli of E_m=(3.52−0.0034T)GPa in which T=T_0+ΔT and T_0=300K (room temperature). In addition, (10, 10) SWCNTs are selected as reinforcements with the

Table 1 Temperature-dependent material properties of (10, 10) SWCNT (L=9.26 nm, R=0.68 nm, h=0.067 nm, υ_{12}^{CNT}=0.175)

Temperature (K)	$E_{11}^{CNT}(TPa)$	$E_{22}^{CNT}(TPa)$	$G_{12}^{CNT}(TPa)$	$\alpha_{12}^{CNT}(10^{-6}/K)$	$\alpha_{22}^{CNT}(10^{-6}/K)$
300	5.6466	7.0800	1.9445	3.4584	5.1682
500	5.5308	6.9348	1.9643	4.5361	5.0189
700	5.4744	6.8641	1.9644	4.6677	4.8943

Table 2 Dimensionless buckling load parameter for various types of CNTRC plates and different loading type

Mode	Loading type	Type of CNTRC, Lei *et al*. (2013)			Type of CNTRC, Present work		
		UD	FGO	FGX	UD	FGO	FGX
1	χ_1=−1, χ_2=0	30.9076	18.7534	40.8005	30.9075	18.7531	40.8003
	χ_1=−1, χ_2=−1	9.3805	6.9161	11.4231	9.3804	6.9157	11.4229
	χ_1=−1, χ_2=1	89.9909	63.4215	104.9802	89.9906	63.4208	104.9800
2	χ_1=−1, χ_2=0	46.9779	34.4733	57.3978	46.9768	34.4727	57.3969
	χ_1=−1, χ_2=−1	10.3981	8.9197	11.6524	10.3977	8.9189	11.6519
	χ_1=−1, χ_2=1	101.0670	81.0655	108.9411	101.0661	81.0644	108.9402
3	χ_1=−1, χ_2=0	69.3855	48.4971	82.0077	69.3846	48.4961	82.0066
	χ_1=−1, χ_2=−1	14.0470	9.3380	15.0540	14.0468	9.3375	15.0534
	χ_1=−1, χ_2=1	107.7075	92.2314	113.8593	107.7066	92.2301	113.8581

material properties listed in Table 1. The elastomeric medium is made of Poly dimethylsiloxane (PDMS) which the temperature-dependent material properties of which are assumed to be v_s=0.48 and E_s=(3.22−0.0034T)GPa in which T=T_0+ΔT and T_0=300K (room temperature) (Shen 2009).

4.1 Validation

To demonstrate the validity of this work, present results are compared with those reported by Lei *et al.* (2013). For this purpose, ignoring the nonlinear terms in governing equations, nonlocal parameter and elastomeric medium, the non-dimensional buckling load parameter (i.e., $\overline{N}_{cr}=N_{cr}L_y^2/E_mh^3$) of the CNTRC plate with simply supported boundary condition is shown in Table 2 considering material properties the same as Lei *et al*. (2013). Three loading types are considered namely as uniaxial compression (i.e., χ_1=−1, χ_2=0), biaxial compression (i.e., χ_1=−1, χ_2=−1) and biaxial compression and tension (i.e., χ_1=−1, χ_2=1). As can be seen, present results obtained by GDQM are in good agreement with those reported by Lei *et al*. (2013) based on the element-free kp-Ritz method. It is noted that a little difference between the results of Lei *et al*. (2013) and present work is due to the different methods for solution.

4.2 Nonlinear buckling of CNTRC microplate

In the following figures, dimensionless buckling load of CNTRC microplate (i.e., $\overline{N}=N_{ii}^M/E_mh(i=x,y)$) in the case of biaxial compression is plotted against nonlocal parameter for different parameters.

The convergence and accuracy of the DQM in evaluating the nonlinear buckling load of the CNTRC micro plates is shown in Fig. 2. The results are prepared for different values of the DQM

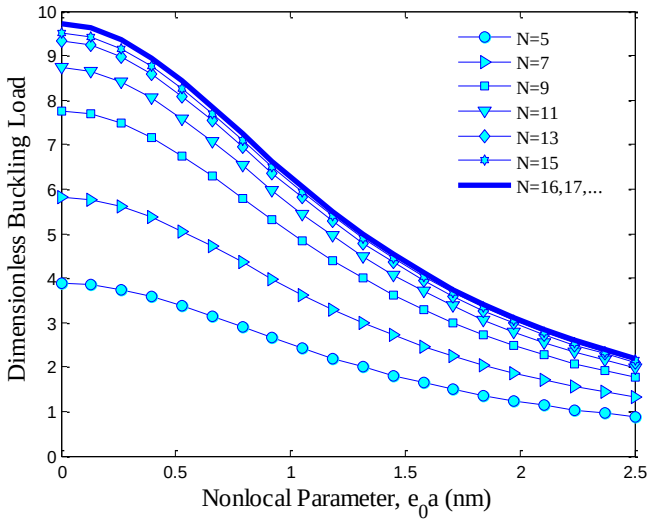

Fig. 2 Convergence and accuracy of DQM

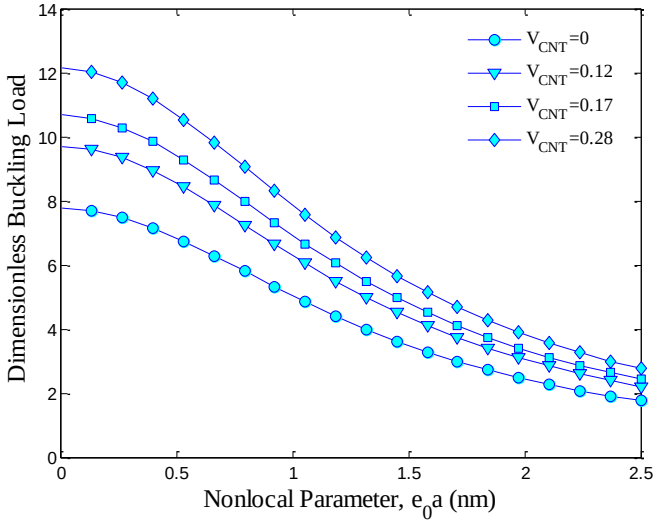

Fig. 3 Effects of CNT volume fraction on the nonlinear buckling behavior of CNTRC plates

grid points. Fast rate of convergence of the method are quite evident and it is found that fifteen DQ grid points can yield accurate results.

Fig. 3 illustrates the effect of the SWCNT volume fraction on the buckling load of the CNTRC microplate versus nonlocal parameter. As can be seen increasing the nonlocal parameter decreases the buckling load. This is due to the fact that the increase of nonlocal parameter decreases the interaction force between microplate atoms, and that leads to a softer structure. It is also found that increasing the CNT volume fraction increases the buckling load of the CNTRC microplate. This is due to the fact that the increase of CNT volume fraction leads to a harder structure. Meanwhile, the effect of CNT volume fraction becomes more considerable at lower nonlocal parameters.

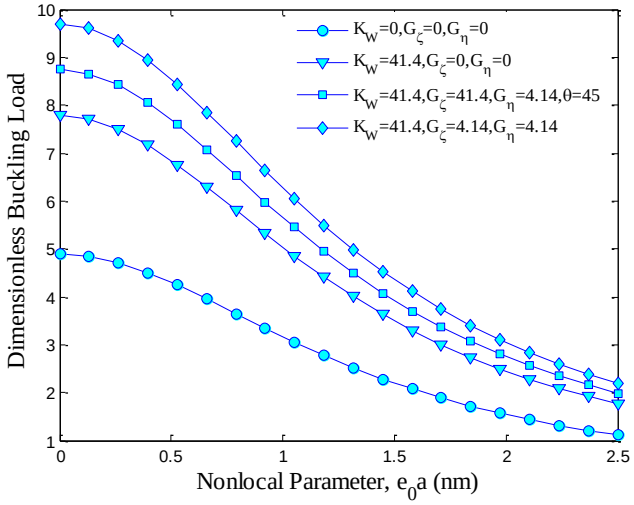

Fig. 4 Effects of elastomeric medium on the nonlinear buckling behavior of CNTRC plates

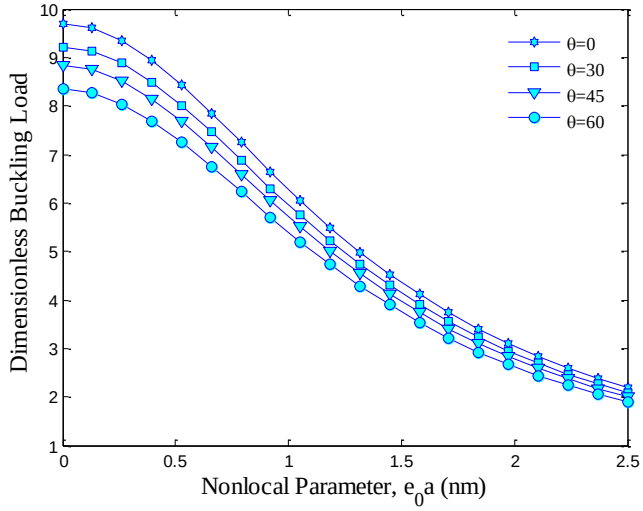

Fig. 5 Effects of orientation of foundation orthtotropy direction on the nonlinear buckling behavior of CNTRC plates

The buckling load of the CNTRC microplate versus nonlocal parameter is demonstrated in Fig. 4 for different elastomeric temperature-dependent mediums. In this figure, four cases are considered as follows

Case 1: K_W=0 N/m^3, G_ξ=0 N/m, G_η=0 N/m→indicating without elastomeric medium.

Case 2: K_W=41.4 N/m^3, G_ξ=0 N/m, G_η=0 N/m→indicating elastomeric Winkler medium.

Case 3: K_W=41.4 N/m^3, G_ξ=4.14 N/m, G_η=4.14 N/m→indicating elastomeric Pasternak medium.

Case 4: K_W=41.4 N/m^3, G_ξ=41.4 N/m, G_η=4.14 N/m, θ=45°→indicating elastomeric orthotropic Pasternak medium.

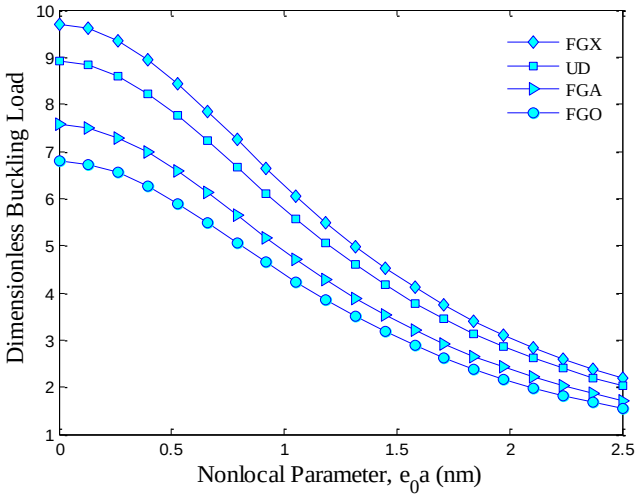

Fig. 6 Effects of CNT distribution on the nonlinear buckling behavior of CNTRC plates

As can be seen, considering elastomeric medium increases buckling load of the CNTRC microplate. It is due to the fact that considering elastomeric medium leads to stiffer structure. Furthermore, the effect of the elastomeric Pasternak-type is higher than the elastomeric Winkler-type on the buckling load of the CNTRC microplate. It is perhaps due to the fact that the elastomeric Winkler-type is capable to describe just normal load of the elastomeric medium while the elastomeric Pasternak-type describes both transverse shear and normal loads of the elastomeric medium.

The effect of the orientation of foundation orthtotropy direction on the buckling load of the CNTRC microplate versus nonlocal parameter is depicted in Fig. 5. Noted that in this figure, the foundation parameters are chosen as K_W=41.4 N/m^3, G_ξ=41.4 N/m, and G_η=4.14 N/m. As can be seen, the buckling load of the CNTRC microplate decreases with increasing orientation of foundation orthtotropy direction. Meanwhile, the effect of orientation of foundation orthtotropy direction on the buckling of the CNTRC microplate becomes more prominent at lower nonlocal parameters.

Fig. 6 illustrates the effect of SWCNT distribution in microplate on the buckling load of the CNTRC microplate versus nonlocal parameter. For the CNTRC microplate, UD and three types of FG distribution patterns of SWCNT reinforcements are assumed. It should be noted that the mass fraction (w_{CNT}) of the UD and FG distribution of CNTs in polymer are considered equal for the purpose of comparisons. As can be seen, the buckling load of FGA- and FGO- CNTRC microplates are lower than the buckling load of UD-CNTRC plates while the FGX- CNTRC microplate have higher buckling load with respect to three other cases. It is due to the fact that the stiffness of CNTRC microplates changes with the form of CNT distribution in matrix. However, it can be concluded that SWCNT distribution close to top and bottom are more efficient than those distributed nearby the mid-plane for increasing the stiffness of plates.

Fig. 7 shows the buckling load of the CNTRC microplate versus nonlocal parameter for different temperature gradients. The same as other figures, increasing the nonlocal parameter decreases the buckling load of the CNTRC microplate. It can be also found that the buckling load of the CNTRC microplate decreases with increasing temperature which is due to the higher

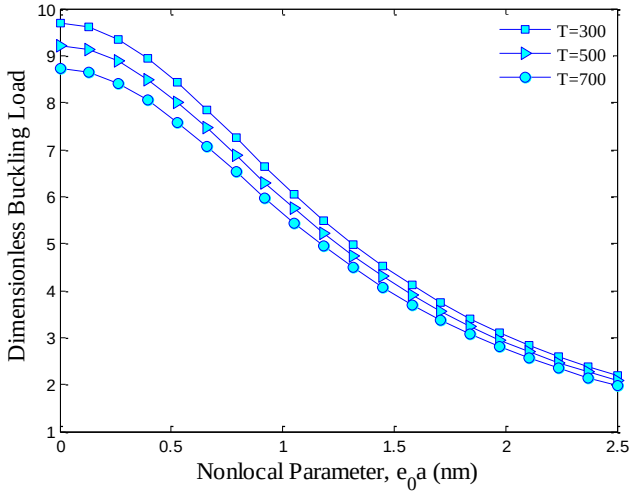

Fig. 7 Effects of temperature on the nonlinear buckling behavior of CNTRC plates

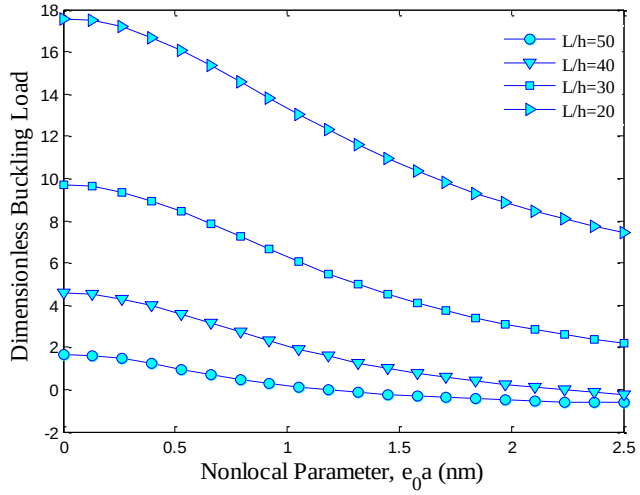

Fig. 8 Effects of slenderness ratio on the nonlinear buckling of CNTRC plates

stiffness CNTRC microplate with lower temperature.

The effect of the slenderness ratio on buckling load of the CNTRC microplate versus nonlocal parameter is depicted in Fig. 8. As can be seen, the buckling load of the CNTRC microplate decreases with increasing slenderness ratio. It is because that increasing slenderness ratio leads softer structure. Meanwhile, the effect of slenderness ratio on the buckling of the CNTRC microplate becomes more prominent at lower nonlocal parameters.

Fig. 9 shows the buckling load of the CNTRC microplate versus nonlocal parameter for different boundary conditions. It can be observed that the buckling load of microplate with CCCC boundary condition is greater than those of plates with SSSS boundary condition and also the buckling load of SCSC microplate is between the buckling load of microplate with the two other

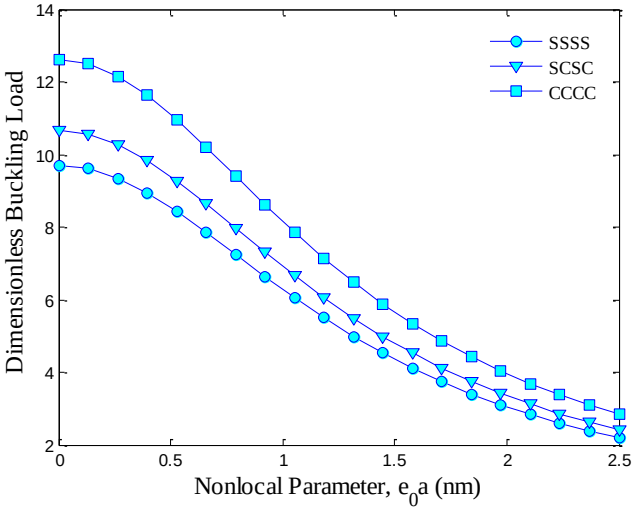

Fig. 9 Effects of different boundary condition on the nonlinear buckling of CNTRC plates

boundary conditions. This is due to the fact that the CNTRC microplate with CCCC boundary condition has higher stiffness with respect to other boundary conditions.

5. Conclusions

Nonlocal nonlinear buckling analysis of an embedded CNTRC microplate was studied in this paper based on orthotropic temperature-dependent Mindlin polymeric microplate and Eringen's theories. CNT distributions in polymer were considered as UD, FGA, FGX and FGO. The rule of mixture was used for obtaining the material properties of FG-CNTRC plate. The FG-CNTRC was surrounded in an orthotropic temperature-dependent elastomeric medium. Using strain-displacement relation, energy method and Hamilton's principle, the governing equations were derived in which the small scale effects are incorporated. In order to obtain the buckling load of the FG-CNTRC plate plate, GDQM was performed. The effects of the volume fractions of carbon nanotubes, elastomeric medium, aspect ratio, orientation of foundation orthtotropy direction, temperature and boundary conditions were considered. Results indicate that considering elastomeric medium increases buckling load of the FG-CNTRC microplate. Furthermore, the lowest and highest buckling load was respectively obtained for FGX- and FGO-CNTRC microplates in the case of constant slenderness ratio and SWCNT volume fraction.

References

Ahmadi, A.R., Farahmand, H. and Arabnejad, S. (2012), "Buckling analysis of rectangular flexural microplates using higher continuity p-version finite-element method", *Int. J. Multisc. Computat. Eng.*, **10**, 249-259.

Akhavan, H., Hosseini Hashemi, Sh., Rokni Damavandi Taher, H., Alibeigloo, A. and Vahabi, Sh. (2009a), "Exact solutions for rectangular Mindlin plates under in-plane loads resting on Pasternak elastic

foundation. Part I: Buckling analysis", *Comput. Mat. Sci.*, **44**, 968-978.
Akhavan, H., Hosseini Hashemi, Sh., Rokni Damavandi Taher, H., Alibeigloo, A. and Vahabi, Sh. (2009b), "Exact solutions for rectangular Mindlin plates under in-plane loads resting on Pasternak elastic foundation. Part II: Frequency analysis" *Comput. Mat. Sci.*, **44**, 951-961.
Baltacıoğlu, A.K., Civalek, Ö., Akgöz, B. and Demir, F. (2011), "Large deflection analysis of laminated composite plates resting on nonlinear elastic foundations by the method of discrete singular convolution", *Int. J. Pres. Ves. Pip.*, **88**, 290-300.
Chen, W. (1996), *Differential Quadrature Method and its Applications in Engineering*, Shanghai Jiao Tong University.
Civalek, Ö. (2004), "Application of differential quadrature (DQ) and harmonic differential quadrature (HDQ) for buckling analysis of thin isotropic plates and elastic columns", *Eng. Struct.*, **26**, 171-186.
Eringen, A.C. (1972), "Nonlocal polar elastic continua", *Int. J. Eng. Sci.*, **10**, 1-16.
Esawi, A.M.K. and Farag, M.M. (2007), "Carbon nanotube reinforced composites: potential and current challenges", *Mater. Des.*, **28**, 2394-2401.
Farahmand, H., Ahmadi, A.R. and Arabnejad, S. (2011), "Thermal buckling analysis of rectangular microplates using higher continuity p-version finite element method", *Thin Wall. Struct.*, **49**, 1584-1591.
Ferreira, A.J.M., Roque, C.M.C. and Martins, P.A.L.S. (2003), "Analysis of composite plates using higher-order shear deformation theory and a finite point formulation based on the multiquadric radial basis function method", *Compos. Part B*, **34**, 627-636.
Jafari Mehrabadi, S., Sobhani Aragh, B., Khoshkhahesh, V. and Taherpour, A. (2012), "Mechanical buckling of nanocomposite rectangular plate reinforced by aligned and straight single-walled carbon nanotubes", *Compos. Part B: Eng.*, **43**, 2031-2040.
Fiedler, B., Gojny, F.H., Wichmann, M.H.G., Nolte, M.C.M. and Schulte, K. (2006), "Fundamental aspects of nano-reinforced composites", *Compos. Sci. Technol.*, **66**, 3115-3125.
Kim, S.M. (2004), "Buckling and vibration of a plate on elastic foundation subjected to in-plane compression and moving loads", *Int. J. Solid. Struct.*, **41**, 5647-5661.
Kutlu, A. and Omurtag, M.H. (2012), "Large deflection bending analysis of elliptic plates on orthotropic elastic foundation with mixed finite element method", *Int. J. Mech. Sci*., **65,** 64-74.
Lei, Z.X., Liew, K.M. and Yu J.L. (2013), "Buckling analysis of functionally graded carbon nanotube-reinforced composite plates using the element-freekp-Ritz method", *Compos. Struct.*, **98**, 160-168.
Morozov, N.F. and Tovstik, P.E. (2010), "On modes of buckling for a plate on an elastic foundation", *Mech. Solid*., **45**, 519-528.
Reddy, J.N. (1984), "A simple higher order theory for laminated composite plates", *J. Appl. Mech.*, **51,** 745-752.
Salvetat-Delmotte, J.P. and Rubio, A. (2002), "Mechanical properties of carbon nanotubes: a fiber digest for beginners", *Carbon*, **40**, 1729-1734.
Shahba, A. and Rajasekaran, S. (2012), "Free vibration and stability of tapered Euler-Bernoulli beams made of axially functionally graded materials", *Appl. Math. Model.*, **36**, 3094-3111.
Shen, H.S. (2009), "Nonlinear bending of functionally graded carbon nanotube-reinforced composite plates in thermal environments", *Compos. Struct.*, **91**, 9-19.
Shen, H.S. and Zhang, C.L. (2011), "Nonlocal beam model for nonlinear analysis of carbon nanotubes on elastomeric substrates", *Comput. Mat. Sci.*, **50**, 1022-1029.
Shu, C. (1999), *Differential Quadrature and its Application in Engineering*, Springer.
Swaminathan, K. and Ragounadin, D. (2004), "Analytical solutions using a higher-order refined theory for the static analysis of antisymmetric angle-ply composite and sandwich plates", *Compos. Struct.*, **64**, 405-417.
Wattanasakulpong, N., Gangadhara Prusty, B., Kelly, D.W. and Hoffman, M. (2012), "Free vibration analysis of layered functionally graded beams with experimental validation", *Mater. Des.*, **36**, 182-190.